Charge disproportionation and interchange transitions in twelve-layer $BaFeO_3$

Zhenhong Tan,[1] Fabio Denis Romero,[1,2] Takashi Saito,[1,3] Masato Goto,[1] Midori Amano Patino,[1] Anucha Koedtruad,[1] Yoshihisa Kosugi,[1] Wei-Tin Chen,[4] Yu-Chun Chuang,[5] Hwo-Shuenn Sheu,[5] J. Paul Attfield,[6] and Yuichi Shimakawa[1,*]

[1]*Institute for Chemical Research, Kyoto University, Uji, Kyoto 611-0011, Japan*

[2]*Hakubi Center for Advanced Research, Kyoto University, Yoshida-honmachi, Sakyo-ku, Kyoto 606-8501, Japan*

[3]*High Energy Accelerator Research Organization (KEK), Tokai, Ibaraki 319-1106, Japan*

[4]*Center for Condensed Matter Sciences and Center of Atomic Initiative for New Materials, National Taiwan University, No. 1, Sec. 4, Roosevelt Road, Taipei 10617, Taiwan*

[5]*National Synchrotron Radiation Research Center, 101 Hsin-Ann Road, Hsinchu Science Park, Hsinchu 30076, Taiwan*

[6]*Center for Science at Extreme Conditions and School of Chemistry, University of Edinburgh, Mayfield Road, Edinburgh EH9 3JZ, United Kingdom*

(Received 12 June 2020; accepted 13 July 2020; published 3 August 2020)

A fully oxygenated hexagonal 12-layer perovskite $BaFeO_3$ with nominal Fe^{4+} was obtained by high-pressure synthesis. The structure consists of face-sharing Fe_3O_9 octahedral trimers and corner-sharing octahedra. A remarkable series of electronic transitions that relieve the electronic instability of Fe^{4+} are discovered on cooling; $2Fe^{4+} \rightarrow Fe^{3+} + Fe^{5+}$ charge disproportionation and ordering over two sites accompanied by a structural distortion at 500 K; charge disproportionation of the remaining Fe^{4+} with magnetic order at 280 K; and an unprecedented charge interchange where Fe^{3+} and Fe^{5+} states are exchanged between two sites with spin orientation change at 50 K. These properties demonstrate the presence of multiple competing ground states in this complex, highly condensed network of corner- and face-sharing octahedra.

DOI: 10.1103/PhysRevB.102.054404

I. INTRODUCTION

Compounds containing unusually high valence iron ions often show charge disproportionation and charge-transfer transitions to relieve electronic instability, sometimes accompanied by simultaneous changes in structural, transport, and magnetic properties. In $CaFeO_3$, for example, Fe^{4+} shows charge disproportionation ($Fe^{4+} \rightarrow 0.5Fe^{3+} + 0.5Fe^{5+}$) at 290 K, and the rocksalt order of resultant Fe^{3+} and Fe^{5+} leads to a metal-insulator transition [1]. The Bi-doped compound $Ca_{0.5}Bi_{0.5}FeO_3$ containing $Fe^{3.5+}$ undergoes successive charge transitions, and the competing magnetic interactions between Fe spins produce an idle spin state of $Fe^{4.5+}$ in the charge disproportionated phase [2,3]. In quadruple perovskite $LaCu_3Fe_4O_{12}$, on the other hand, $Fe^{3.75+}$ participates in an intersite charge-transfer transition ($3Cu^{2+} + 4Fe^{3.75+} \rightarrow 3Cu^{3+} + 4Fe^{3+}$) at 393 K, and large negative thermal expansion, metal-to-insulator, and paramagnetic-to-antiferromagnetic changes occur simultaneously. These drastic changes in the properties of the charge-lattice-spin coupled system originate from strong hybridization of low-lying Fe-3*d* and O-2*p* orbitals in corner-sharing FeO_6 octahedra [4,5].

Among compounds containing the high valent Fe ions, $BaFeO_3$ is of particular interest because several polymorphic phases with differently connected $Fe^{4+}O_6$ octahedra are known [6]. Furthermore, no apparent charge transitions have been reported in any of the polymorphs to date. The simple cubic perovskite $BaFeO_3$, which is synthesized by low-temperature topochemical oxidation of $BaFeO_{2.5}$, consists of cubic close-packed layers (*c*) in a stacking sequence …*ccc*…(3*C*), as shown in Fig. 1(a). 3*C* $BaFeO_3$ has a spiral spin structure below 111 K but no charge disproportionation was reported [7]. When $BaFeO_3$ is synthesized at high temperature and ambient pressure, the six-layer hexagonal [6*H*, Fig. 1(b)] polymorph is obtained. This consists of corner-sharing and face-sharing octahedra with the stacking sequence of …*cchcch*… (*h* = hexagonal close-packed layer) [8,9]. Fully stoichiometric 6*H* $BaFeO_3$ is difficult to obtain under these conditions, however, and the resulting $BaFeO_{3-\delta}$ containing both Fe^{3+} and Fe^{4+} does not show any charge transition at temperatures down to 4 K [10], and reports on magnetic properties are inconsistent [11–16], probably due to varying oxygen deficiencies of the samples. A rhombohedral 12-layer compound (12*R*) with the stacking sequence …*cchhcchhcchh*… [Fig. 1(c)] was also reported in oxygen-deficient $BaFeO_{3-\delta}$ ($\delta \sim 0.1$) obtained by high-pressure and high-temperature oxidation of brownmillerite $BaFeO_{2.5}$ [17–20]. The structure can also be considered as one where additional *h* layers are introduced into the 6*H* $BaFeO_3$ arrangement. Although magnetic properties were reported [21], details of the magnetic structure and the charge distribution were not determined.

Here, we have investigated the structural and magnetic properties of fully oxygen stoichiometric $BaFeO_3$ containing unusually high valence Fe^{4+} leading to the discovery of a remarkable sequence of electronic and magnetic transitions including an unprecedented charge interchange between ordered Fe^{3+} and Fe^{5+} states.

*Corresponding author: shimak@scl.kyoto-u.ac.jp

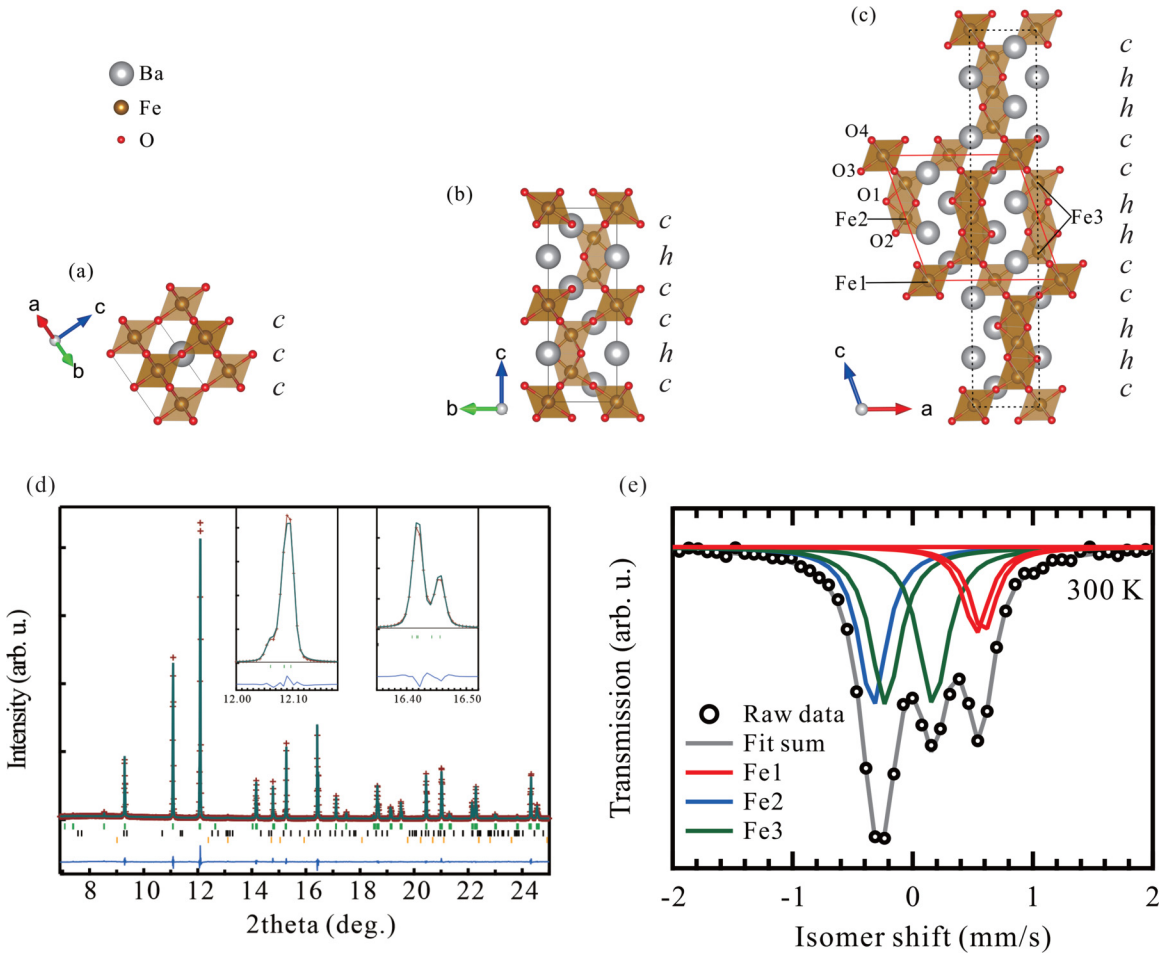

FIG. 1. Crystal structures of (a) 3*C*, (b) 6*H*, and (c) 12-layer $BaFeO_3$. Dashed black and red lines in (c) indicate $R\bar{3}m$ rhombohedral and $C2/m$ monoclinic unit cells, respectively. (d) Rietveld fit to SXRD data obtained at room temperature with the wavelength of 0.599 86 Å using a monoclinic ($C2/m$) structure model. The top (green), middle (black), and bottom (orange) vertical tick marks represent the Bragg peak positions of monoclinic 12-layer $BaFeO_3$ (97.64 wt %), $BaCO_3$ (1.87 wt %), and α-Fe_2O_3 (0.49 wt %), respectively. The insets show the splitting of selected diffraction peaks of $BaFeO_3$. (e) Fitted ^{57}Fe Mössbauer spectra of 12-layer $BaFeO_3$ at room temperature.

II. EXPERIMENTAL DETAILS

Synthesis. Precursor 6*H* $BaFeO_{3-\delta}$ ($\delta \sim 0.3$) was prepared by solid-state reaction of $BaCO_3$ and Fe_2O_3 at 1273 K for 12 h in an oxygen atmosphere. It was then mixed with the oxidizing agent $KClO_4$, sealed into a platinum capsule, placed in a cubic-anvil-type high-pressure apparatus, and treated at 2–4 GPa and 1273 K for 30 min. After the high-pressure treatment, the sample was quenched to room temperature and the pressure was released. The sample was then washed with distilled water to remove the KCl and unreacted $KClO_4$.

Characterization. The samples obtained under different conditions were characterized by x-ray diffraction (XRD). Detailed crystal structures of $BaFeO_3$ prepared at 3 GPa were analyzed by using synchrotron x-ray diffraction (SXRD) data collected at TPS09A in NSRRC ($\lambda = 0.826\,56$ Å) and BL02B2 in SPring-8 ($\lambda = 0.599\,86$ Å). The powder sample was filled into a 0.2-mm silica capillary tube and the tube was rotated during the measurement to minimize the absorption. Temperature-dependent SXRD data in the temperature range 300–1073 K were collected at TPS09A, and those in the range 100–700 K were collected at BL02B2. The crystal structure parameters were refined by the Rietveld method with the computer program RIETAN-FP [22,23], and the crystal structure models were drawn by using the software VESTA [24]. Neutron-diffraction (ND) data in the temperature range 4.2–300 K were collected by using the Polaris diffractometer at the ISIS Neutron Source. The powder sample was sealed into a vanadium can. The data were analyzed by using GSAS programs [25]. The valence states of cations in $BaFeO_3$ were calculated using the bond valence sum (BVS) method. The BVS formula is $\mathrm{BVS} = \sum_i e^{(r_0 - r_i)/0.37}$, where r_i represents the bond lengths between a cation and the adjacent oxygen ions [26]. The BVS values for Fe ions were estimated using r_0 values 1.780 [27].

^{57}Fe Mössbauer spectroscopy. ^{57}Fe Mössbauer spectra were measured at various temperatures (5–490 K) in order to investigate the valence and magnetic states of Fe ions in the compound. The powder sample was wrapped with Al foil. Temperature-dependent data were collected with a vacuum cryostat ($T < 300$ K) and a Cu plate apparatus with a ceramic plate heater ($T > 300$ K). The temperature was measured with a Pt thermocouple. The measurements were performed in transmission geometry with a constant-acceleration spec-

TABLE I. Crystallographic parameters of 12-layer $BaFeO_3$ refined from SXRD data collected at 300 K. Space group $C2/m$ (no. 12), $a = 9.859\,80(4)$ Å, $b = 5.699\,89(2)$ Å, $c = 9.898\,10(4)$ Å, and $\beta = 109.523\,6(3)^\circ$. $R_{wp} = 5.16\%$ and $R_p = 3.95\%$. All sites are fully occupied.

Atom	Site	x	y	z	$100 \times U_{iso}$(Å^2)
Ba1	4*i*	0.2877(1)	0	0.8614(1)	0.57(2)
Ba2	4*i*	0.1261(1)	0	0.3806(1)	0.56(2)
Fe1	2*a*	0	0	0	0.81(6)
Fe2	2*d*	0	0.5	0.5	0.45(5)
Fe3	4*i*	0.4068(3)	0	0.2210(2)	0.53(5)
O1	4*i*	0.605(1)	0	0.3747(9)	0.8(3)
O2	8*j*	0.6151(7)	0.220(1)	0.6239(6)	1.2(2)
O3	4*i*	0.791(1)	0	0.875(1)	1.6(3)
O4	8*j*	0.4565(9)	0.252(2)	0.1259(8)	0.5(2)

trometer by using a ^{57}Co /Rh radiation source. The velocity scale and isomer shift (IS) were estimated with the relative values of α-Fe at room temperature. The spectra were fitted to Lorentzian functions by using the standard least-squares method.

Heat-capacity measurement. In order to confirm the phase transition, heat capacity of the synthesized $BaFeO_3$ was measured by using differential scanning calorimetry (DSC 3500 Sirius, NETZSCH). The powder sample was placed in an Al container. The DSC data were collected from 573 to 303 K with a ramp rate of -10 K min^{-1}.

Magnetic property measurements. Magnetic properties of the sample were measured by using a Quantum Design MPMS superconducting quantum interference device magnetometer. The magnetic susceptibility data were collected at temperatures from 300 to 5 K with an applied field of 1 kOe.

III. RESULTS AND DISCUSSION

Oxygen-stoichiometric samples of $BaFeO_3$ were obtained by treating 6*H* $BaFeO_{3-\delta}$ at pressures between 2 and 4 GPa with the oxidizing agent $KClO_4$. We first analyzed the crystal structure at room temperature by powder SXRD. A structural model based on the previously reported $R\bar{3}m$ rhombohedral (12*R*) structure [20] resulted in a poor fit to the data ($R_{wp} =$ 23.50%, Fig. S1 in the Supplemental Material [28]). Better observed and statistical fits were obtained by using a monoclinic structure (space group $C2/m$) shown in Fig. 1(c). This model is a monoclinically distorted variant of the 12*R* structure containing face-sharing trimers. The final refinement results ($R_{wp} = 5.16\%$) are shown in Fig. 1(d) and Table I. The crystal structure analysis with powder neutron diffraction (ND) at room temperature also confirmed the $C2/m$ monoclinic crystal structure (Fig. S2 and Table S1 in the Supplemental Material [28]). All oxygen sites refined to full occupancy within experimental error and thus the compound has the stoichiometric composition. This is in sharp contrast with the occupancy for the previously reported 12*R* $BaFeO_{3-\delta}$ samples which always contain oxygen vacancies. We thus conclude that the present form of $BaFeO_3$ synthesized under highly oxidizing conditions is the fully oxygenated monoclinic structure phase of 12-layer $BaFeO_3$. BVSs calculated from the structure refinement are +3.03 for Fe1 (2*a* site in the corner-sharing octahedra), +4.90 for Fe2 (2*d* site in the face-sharing octahedra), and +3.89 for Fe3 (4*i* site in the corner- and face-sharing octahedra). ^{57}Fe Mössbauer spectra taken at 300 K [Fig. 1(e)] can be fitted with one singlet and two doublets with an area ratio of approximately 1:1:2. The ISs for the corresponding components are +0.559, −0.332, and -0.028 mm s^{-1}, respectively. The first component is typical for Fe^{3+} coordinated by six oxygen ions octahedrally [29]. The second, with large negative IS, suggests an unusually high valence state of Fe, and the signal can be assigned to Fe^{5+} [30]. The last, with the small IS, is similar to those of $CaFe^{4+}O_3$ (IS = 0.073 mm s^{-1}) [1] and $SrFe^{4+}O_3$ (IS = 0.054 mm s^{-1}) [31]. The results thus suggest that at room temperature, the structure contains Fe^{3+}, Fe^{4+}, and Fe^{5+} with the formula $Ba_4Fe1^{3+}Fe2^{5+}Fe3^{4+}{}_2O_{12}$. This demonstrates that Fe^{4+} in the 12-layer $BaFeO_3$ is charge disproportionated over Fe1 and Fe2 sites, but remains undisproportionated at ordering of three different valence states over three different sites.

A possible $Fe1^{3+}/Fe2^{5+}$ charge disproportionation transition above room temperature was investigated by high-temperature SXRD, differential scanning calorimetry (DSC), and Mössbauer spectroscopy. In the temperature-dependent SXRD patterns, significant changes in the diffraction intensity were observed between 480 and 500 K [Figs. 2(a) and 2(b)]. The refinement against SXRD data collected at 570 K resulted in a good fit [$R_{wp} = 4.94\%$, Fig. 2(c)] by using the $R\bar{3}m$ rhombohedral structure model, suggesting a structural transition from the high-temperature rhombohedral ($R\bar{3}m$) to low-temperature monoclinic ($C2/m$) phase. Temperature dependencies of structure parameters (Fig. S3 in the Supplemental Material [28]) and heat-capacity measured in DSC (Fig. S4 in the Supplemental Material [28]) confirm the phase transition at 500 K. Thermogravimetry shows that no change in oxygen stoichiometry occurs at the transition. This phase transition is consistent with a charge disproportionation transition, although a clear change in the Mössbauer spectra was not accessible due to difficulties in performing experiments at temperature over 500 K. The Mössbauer spectrum at 490 K, which is just below the transition temperature, consists of three singlet components of Fe1, Fe2, and Fe3 with the IS +0.268, −0.411, and -0.087 mm s^{-1}, respectively [Fig. 2(d)]. The significant decrease in IS of Fe1 implies an increase of valence state, which is closer to Fe^{4+}. It is therefore reasonable to conclude that the charge disproportionation transition occurs at about 500 K. This transition leads to charge ordering over Fe1 and Fe2 sites; $Ba_4Fe1^{4+}Fe2^{4+}Fe3^{4+}{}_2O_{12} \rightarrow Ba_4Fe1^{3+}Fe2^{5+}Fe3^{4+}{}_2O_{12}$. As indicated by the paramagnetic singlets in the Mössbauer spectra above room temperature, the charge disproportionation transition at 500 K is not associated with the magnetic transition.

A local maximum at 280 K in the temperature dependence of magnetic susceptibility [Fig. 3(a)] suggests an antiferromagnetic transition. Mössbauer spectroscopy data collected below 280 K shown in Fig. 2(e) consist of four sextets, indicating that all Fe spins are magnetically ordered. Importantly, the IS of each spectrum component is +0.419, −0.359, +0.411, and -0.174 mm s^{-1}, and the area ratios are approximately

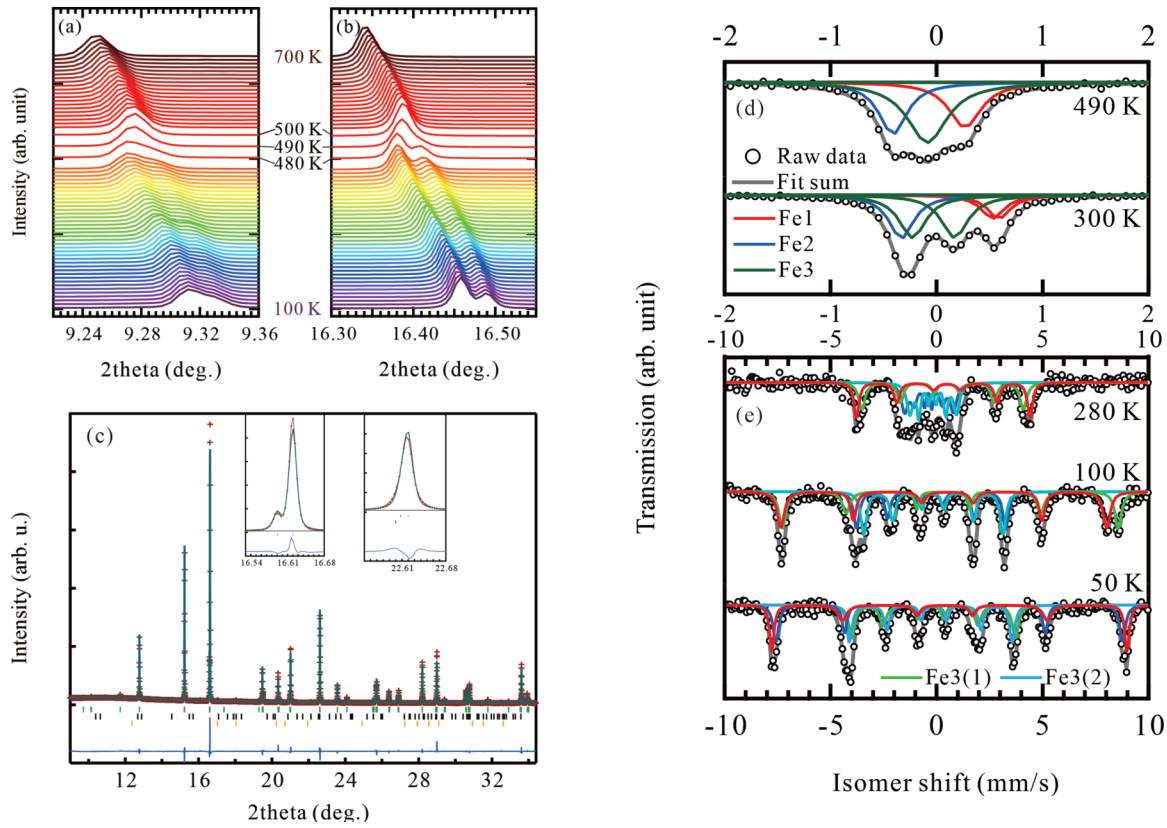

FIG. 2. Temperature-dependent SXRD in 10-K intervals showing splitting of the 12*R* (a) (0 1 5), (b) (1 1 9), and (0 2 7) peaks at the 500 K rhombohedral to monoclinic structural transition. (c) Rietveld fit to SXRD data obtained at 570 K with a wavelength of 0.826 56 Å using a rhombohedral ($R\bar{3}m$) structure model. The top (green), middle (black), and bottom (orange) vertical tick marks represent the Bragg peak positions of rhombohedral $BaFeO_3$ (96.43 wt %), $BaCO_3$ (2.67 wt %), and α-Fe_2O_3 (0.90 wt %), respectively. The insets show the selected diffraction peaks. $a = 5.718\,30(2)$ Å, $c = 28.089\,1(1)$ Å, $R_{wp} = 4.94\%$, and $R_p = 3.11\%$. (d),(e) Fitted ^{57}Fe Mössbauer spectra of 12-layer $BaFeO_3$ at selected temperatures.

1:1:1:1. In comparison to the spectrum at 300 K, the $Fe3^{4+}$ component appears to have split into two sextets consistent with charge disproportionation and ordering that splits the Fe3 site into two subsites, $2Fe3^{4+} \rightarrow Fe3(1)^{3+} + Fe3(2)^{5+}$. The result implies that a second charge disproportionation of Fe in the Fe_3O_9 trimers accompanies the antiferromagnetic order.

Variable temperature SXRD data collected at temperatures below 300 K do not show any further structural transitions (see Fig. S3 in the Supplemental Material [28]). However, variable temperature ND data collected below 280 K show additional reflections consistent with long-range magnetic order [Figs. 3(b)–3(d)]. All magnetic reflections are accounted for using a $1 \times 1 \times 2$ expansion of the nuclear cell. However, two k vectors, (0, 0, 1/2) and (0, 1, 1/2), are needed to fit the observed intensities. The best fit to the data was achieved by using the model shown in Fig. 3(e) in which the Fe1 spins order along (010), Fe2 along $(0\bar{1}0)$, and Fe3 along both (010) and $(0\bar{1}0)$. This combination results in two inequivalent Fe3 sites and hence four Fe sites in 1:1:1:1 ratio overall, consistent with the Mössbauer spectra. The Fe1 spins form ferromagnetic sheets stacked antiferromagnetically while the Fe2 moments form antiferromagnetic sheets stacked antiferromagnetically. At 100–250 K, all moments are aligned along the y direction (perpendicular to the ac plane). The refined magnetic moments are 2.34(9), 0.81(9), 1.85(7), and 1.04(8) μB for Fe1, Fe2, Fe3(1), and Fe3(2) at 250 K, respectively (Fig. S6 and Table S3 in the Supplemental Material [28]). The two Fe3 sites refine to have significantly different moments, which is consistent with the charge disproportionation of $Fe3^{4+}$ to $Fe3(1)^{3+}$ and $Fe3(2)^{5+}$ suggested by the low-temperature Mössbauer results. The arrangement of charge-ordered Fe3(1) and Fe3(2) sites shown in Fig. 3(b) changes the crystal structure symmetry from $C2/m$ to $P2_1/m$ or lower, but no superstructure peaks consistent with loss of C centering are observed in the ND patterns.

At temperatures below 100 K, the data were well fitted by letting the direction of the moments point towards the z axis, while maintaining the same relative arrangement. Figure 3(d) shows the refinement results, giving magnetic moments 4.12(5) for Fe1, 3.6(1) for Fe2, and 2.74(5) undistinguishably for Fe3(1) and Fe3(2) sites at 4.2 K (Table S5 in the Supplemental Material [28]). As shown in Fig. 3(f), Fe1 and Fe2 both order along the z direction while maintaining ferromagnetic and antiferromagnetic layers, respectively. Fe3 orders noncollinearly with a moment direction forming an angle of approximately 45° relative to the direction of Fe1 and Fe2 moments. The refined moment results suggest the corresponding charge states to be $Fe1^{3+}$, $Fe2^{3+}$, $Fe3(1)^{5+}$, and $Fe3(2)^{5+}$. This charge distribution is consistent with the Mössbauer spectrum collected at 50 K, which can be fitted

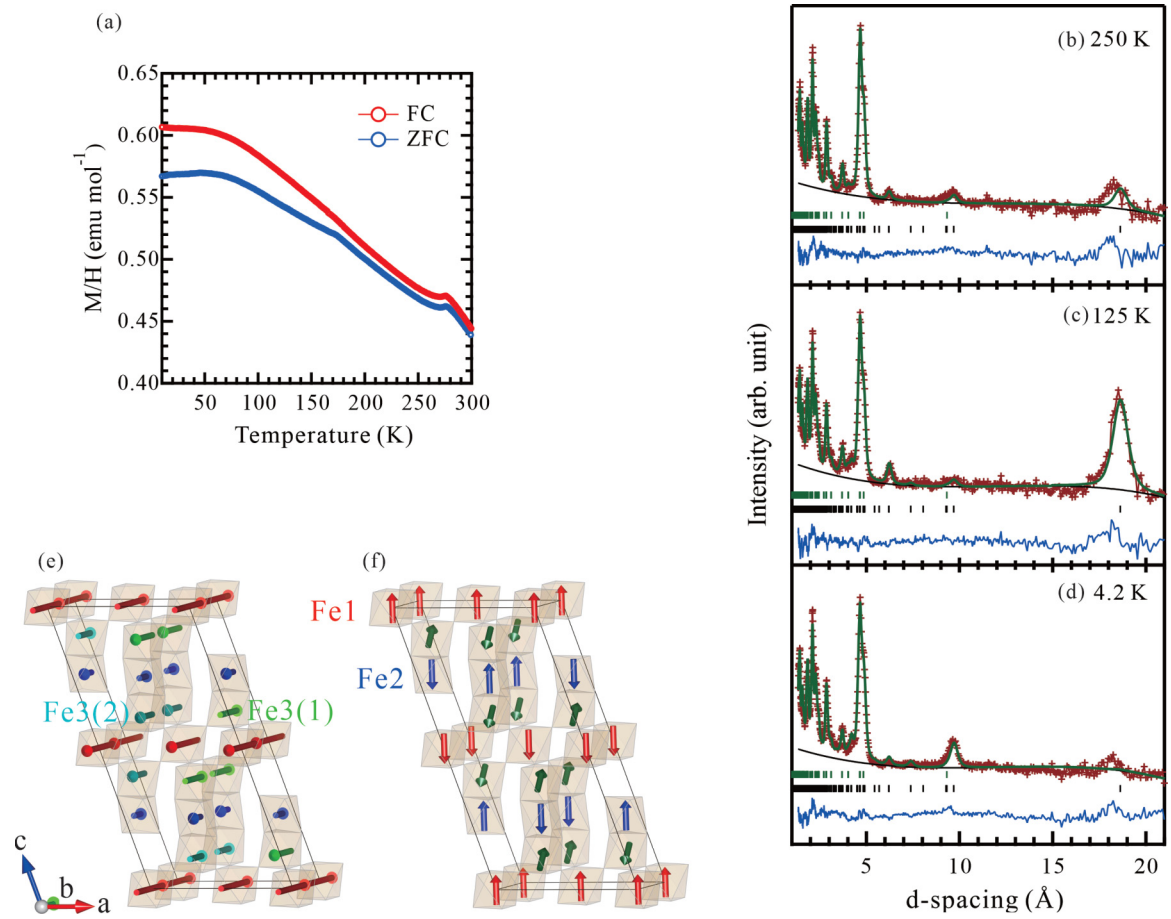

FIG. 3. (a) Temperature dependence of magnetic susceptibility for 12-layer $BaFeO_3$ measured at applied field of 0.1 T. (b)–(d) Rietveld fits to ND patterns of 12-layer $BaFeO_3$ at (b) 250 K, (c) 125 K, and (d) 4.2 K showing changes of long-d peaks due to the evolving spin orders. Results are given in the Supplemental Material [28]. (e),(f) Magnetic structure models for 12-layer $BaFeO_3$ at temperatures (e) between 280 and 100 K, and (f) below 100 K, showing the $1 \times 1 \times 2$ magnetic supercell.

by the four sextets with ISs of +0.498, +0.496, −0.199, and $-0.213\,\mathrm{mm\,s^{-1}}$ [Fig. 2(e)] and is stable down to 4.2 K. Importantly, the ND and Mössbauer results clearly show an intersite charge transfer between Fe2 and Fe3(1) : $Fe2^{5+} + Fe3(1)^{3+} \rightarrow Fe2^{3+} + Fe3(1)^{5+}$, i.e., a valence interchange transition at 50 K (Fig. 4). The large changes of quadruple splitting values for Fe2 and Fe3(1) demonstrate that their chemical environments change during the charge-transfer process. It is also notable that the valence interchange transition is associated with spin reorientation.

The present stoichiometric 12-layer material is the first polymorph of $BaFeO_3$ showing charge disproportionation and ordering transitions, and these are summarized in Fig. 4. The Fe^{4+} charge uniform phase is stable above 500 K in the rhombohedral structure, but its electronic instability results in successive charge-redistributing transitions accompanied by structural and magnetic transitions. The charge-redistributing transitions are discovered to be highly site selective. The first charge disproportionation transition at 500 K occurs at the corner-sharing Fe1 and face-sharing Fe2 sites, but Fe^{4+} remains undisproportionated at the Fe3 site. The second charge transition disproportionates the remaining Fe^{4+} at the Fe3 site. Such successive site-selective charge-disproportionation transitions have not been reported in other materials. The lowest-temperature charge-redistributing transition at 50 K is a valence interchange between the Fe2 and Fe3 sites in the face-sharing octahedral trimers.

In the 12-layer $BaFeO_3$ structure consisting of corner-sharing Fe1 octahedral layers and face-sharing Fe2/Fe3 octahedral trimers, Fe1 is always found to be the largest site and Fe2 the smallest, presumably due to the face-sharing constraints on the Fe2 and Fe3 but not Fe1 sites. This results in the large Fe1 site being occupied by Fe^{3+} cations and the small Fe2 site being occupied by Fe^{5+} cations after the first charge disproportionation transition. Once the Fe3 undergoes the charge disproportionation at the second transition at 280 K, Fe^{5+} ions are close to each other within two face-sharing octahedra inside the trimers. The resulting electrostatic repulsion likely drives the 50-K valence interchange transition that redistributes the charges into an alternating arrangement of Fe^{3+} and Fe^{5+} in the trimers, without direct Fe^{5+}-Fe^{5+} contacts between face-sharing octahedra. The unusually high Fe valence states have strong hybridization of Fe-3d and O-2p orbitals, so the valence interchange can be regarded as redistribution of ligand holes ($\underline{L}$) described as $d^5\underline{L}^2 + d^5 \rightarrow d^5 + d^5\underline{L}^2$ [5,32]. Such redistribution of the ligand holes can easily be induced through the oxygen ions in the face-sharing octahedra. The second charge disproportionation

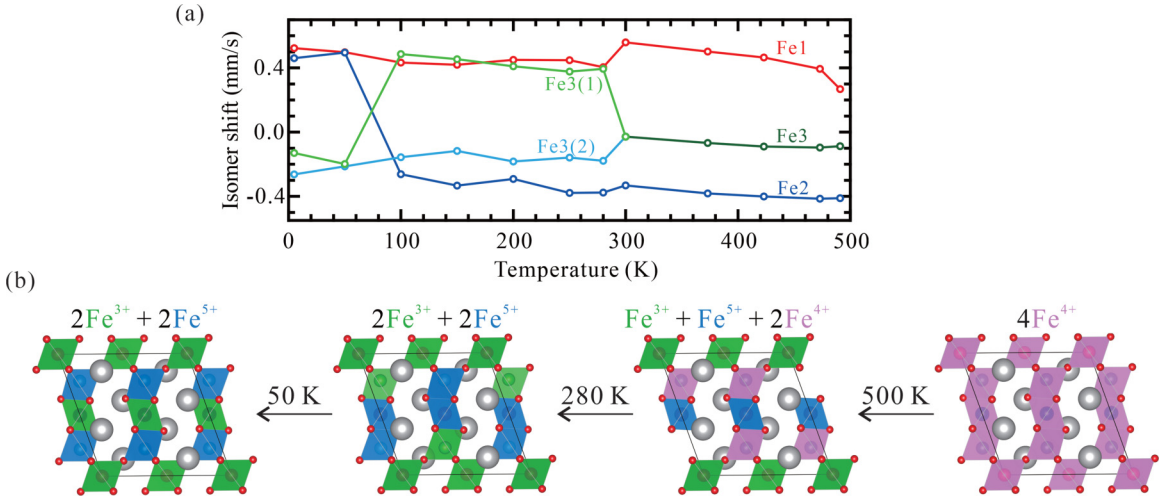

FIG. 4. (a) Plot of isomer shift (IS) fitted from ^{57}Fe Mössbauer spectra of 12-layer $BaFeO_3$ against temperatures showing the electronic transitions at 280 and 50 K. (b) Schematic charge distributions and charge transitions of 12-layer $BaFeO_3$.

transition at 280 K and the charge interchange transition at 50 K respectively are accompanied by the magnetic order and the spin orientation change. The former is a notably high temperature for Fe^{4+} magnetic order, as seen by comparison with the magnetic transitions of Fe^{4+} in $SrFeO_3$ ($T_N = 134$ K) [33] and 3*C* $BaFeO_3$ ($T_c = 111$ K) [7]. The charge order of Fe^{3+} and Fe^{5+} may be important to induce the long-range magnetic order. Below 50 K Fe^{3+}-Fe^{5+} magnetic interactions through between 180° corner-sharing Fe-O-Fe bonds and 90° face-sharing Fe-O-Fe bonds compete, and as a result, a noncollinear magnetic structure is stabilized by the spin orientation change.

IV. SUMMARY

We succeeded in obtaining the oxygenated 12-layer $BaFeO_3$ containing nominal Fe^{4+}, by high-pressure synthesis. From temperature-dependent SXRD, ND, heat capacity, and Mössbauer spectroscopy experiments, we found successive, site-selective charge-redistributing transitions described as $Ba_4Fe1^{4+}Fe2^{4+}Fe3^{4+}{}_2O_{12} \rightarrow$ (500 K) $Ba_4Fe1^{3+}Fe2^{5+}Fe3^{4+}{}_2O_{12} \rightarrow$ (280 K) $Ba_4Fe1^{3+}Fe2^{5+}Fe3(1)^{3+}Fe3(2)^{5+}O_{12} \rightarrow$ (50 K) $Ba_4Fe1^{3+}Fe2^{3+}Fe3(1)^{5+}Fe3(2)^{5+}O_{12}$. The charge disproportionation transition at 500 K occurs at the corner-sharing Fe1 and face-sharing Fe2 sites and is accompanied by a structural transition from rhombohedral ($R\bar{3}m$) to monoclinic ($C2/m$) symmetry. The second charge disproportionation transition at 280 K is of the remaining Fe^{4+} at Fe3 sites and is accompanied by magnetic ordering of all Fe spins. The charge interchange transition between Fe^{3+} and Fe^{5+} states at Fe2 and Fe3 sites at 50 K is accompanied by changes in the spin state and its orientation. Such successive charge disproportionation and interchange transitions with all charges fully ordered in each phase may result from the presence of both corner-sharing and face-sharing octahedra. The 12-layer $BaFeO_3$ demonstrates possibilities within the rich variety of transitions in charge-lattice-spin coupled systems.

ACKNOWLEDGMENTS

We thank D. Kan for helpful discussions. We also thank S. Kawaguchi for help in the SXRD experiments at SPring-8 and thank R. Smith for help in the ND experiments at ISIS Neutron Source. The synchrotron radiation experiments were performed at the Japan Synchrotron Radiation Research Institute (Proposal No. 2019B1757) and the National Synchrotron Radiation Research Center (Proposal No. 2019-1-198). This work was partly supported by Grants-in-Aids for Scientific Research (Grants No. 16H02266, No. 19H05823, and No. 20H00397) and by grants for the Integrated Research Consortium on Chemical Sciences and the International Collaborative Research Program of Institute for Chemical Research in Kyoto University from the Ministry of Education, Culture, Sports, Science and Technology (MEXT) of Japan. This work was also supported by Japan Society for the Promotion of Science (JSPS) Core-to-Core Program (A) Advanced Research Networks and by the Yazaki Memorial Foundation for Science and Technology. Support was also provided by EPSRC and the Royal Society, UK.

Z.T. and Y.S. conceived the idea and initiated the project. Y.S. supervised the project. Z.T., T.S., M.G., and Y.K. prepared the samples and performed the property measurements. Z.T., F.D.R., M.A.P., J.P.A., and Y.S. conducted neutron-diffraction experiments and analyzed the structures as well as magnetic structures. Z.T., M.G., M.A.P., A.K, Y.K., W.-T.C., Y.-C.C., H.-S.S., and Y.S. conducted synchrotron diffraction experiments and analyzed the data. All authors discussed the experimental results. Z.T., F.D.R., J.P.A., and Y.S. mainly wrote the manuscript.

[1] M. Takano, N. Nakanishi, Y. Takeda, S. Naka, and T. Takada, Mater. Res. Bull. **12**, 923 (1977).

[2] Y. Hosaka, F. D. Romero, N. Ichikawa, T. Saito, and Y. Shimakawa, Angew. Chem. Int. Ed. **56**, 4243 (2017).

[3] F. Denis Romero, Y. Hosaka, N. Ichikawa, T. Saito, G. McNally, J. P. Attfield, and Y. Shimakawa, Phys. Rev. B **96**, 064434 (2017).
[4] Y. W. Long, N. Hayashi, T. Saito, M. Azuma, S. Muranaka, and Y. Shimakawa, Nature (London) **458**, 60 (2009).
[5] Y. Shimakawa, J. Phys. Appl. Phys. **48**, 504006 (2015).
[6] S. Mori, J. Am. Ceram. Soc. **49**, 600 (1966).
[7] N. Hayashi, T. Yamamoto, H. Kageyama, M. Nishi, Y. Watanabe, T. Kawakami, Y. Matsushita, A. Fujimori, and M. Takano, Angew. Chem. Int. Ed. **50**, 12547 (2011).
[8] W. W. Malinofsky and H. Kedesdy, J. Am. Chem. Soc. **76**, 3090 (1954).
[9] J. B. MacChesney, J. F. Potter, R. C. Sherwood, and H. J. Williams, J. Chem. Phys. **43**, 3317 (1965).
[10] P. K. Gallagher, J. B. Macchesney, and D. N. E. Buchanan, J. Chem. Phys. **43**, 516 (1965).
[11] F. Iga, Y. Nishihara, T. Katayama, K. Murata, and Y. Takeda, J. Magn. Magn. Mater. **104-107**, 1973 (1992).
[12] F. Iga, Y. Nishihara, and Y. Takeda, J. Magn. Magn. Mater. **104-107**, 1969 (1992).
[13] K. Mori, T. Kamiyama, H. Kobayashi, K. Oikawa, T. Otomo, and S. Ikeda, J. Phys. Soc. Jpn. **72**, 2024 (2003).
[14] S. Morimoto, K. Kuzushita, and S. Nasu, J. Magn. Magn. Mater. **272-276**, 127 (2004).
[15] I. Gil de Muro, M. Insausti, L. Lezama, and T. Rojo, J. Solid State Chem. **178**, 1712 (2005).
[16] K. Mori, T. Kamiyama, H. Kobayashi, T. Otomo, K. Nishiyama, M. Sugiyama, K. Itoh, T. Fukunaga, and S. Ikeda, J. Appl. Crystallogr. **40**, s501 (2007).
[17] C. Gleitzer and M. Zanne, C. R. Acad. Sci. Paris Ser. C **267**, 1601 (1968).
[18] M. Zanne and C. Gleitzer, Bull. Soc. Chim. Fr. **1971**, 1567 (1971).
[19] Y. Takeda, M. Shimada, F. Kanamaru, and M. Koizumi, J. Solid State Chem. **7**, 229 (1973).
[20] M. Parras, M. Vallet-Regi, J. M. Gonzalez-Calbet, J. C. Grenier, P. Hagenmuller, and J. Rodriguez-Carvajal, Eur. J. Solid State Inorg. Chem. **26**, 299 (1989).
[21] Y. Takeda, M. Shimada, F. Kanamaru, M. Koizumi, and N. Yamamoto, Mater. Res. Bull. **9**, 537 (1974).
[22] H. M. Rietveld, J. Appl. Crystallogr. **2**, 65 (1969).
[23] F. Izumi and K. Momma, Solid State Phenom. **130**, 15 (2007).
[24] K. Momma and F. Izumi, J. Appl. Crystallogr. **44**, 1272 (2011).
[25] A. C. Larson and R. B. Von Dreele, Los Alamos Natl. Lab. Rep. LAUR 86-748, 2000.
[26] I. D. Brown and D. Altermatt, Acta Crystallogr., Sect. B **41**, 244 (1985).
[27] N. E. Brese and M. O'Keeffe, Acta Crystallogr., Sect. B **47**, 192 (1991).
[28] See Supplemental Material at http://link.aps.org/supplemental/10.1103/PhysRevB.102.054404 for Rietveld fits for SXRD patterns by using different space groups for 12-layer $BaFeO_3$; Rietveld fits for ND patterns at 300 K; Rietveld refinement results for SXRD patterns obtained at temperatures from 100 to 700 K; heat capacity measurement; magnetic structure and Rietveld fits for ND patterns and results at 4.2, 125 and 250 K.
[29] P. Gütlich, E. Bill, and A. Trautwein, in *Mössbauer Spectroscopy and Transition Metal Chemistry: Fundamentals and Application* (Springer, Berlin, 2011).
[30] P. Xiong, H. Seki, H. C. Guo, Y. Hosaka, T. Saito, M. Mizumaki, and Y. Shimakawa, Inorg. Chem. **55**, 6218 (2016).
[31] P. K. Gallagher, J. B. MacChesney, and D. N. E. Buchanan, J. Chem. Phys. **41**, 2429 (1964).
[32] A. E. Bocquet, A. Fujimori, T. Mizokawa, T. Saitoh, H. Namatame, S. Suga, N. Kimizuka, Y. Takeda, and M. Takano, Phys. Rev. B. **45**, 1561 (1992).
[33] J. B. MacChesney, R. C. Sherwood, and J. F. Potter, J. Chem. Phys. **43**, 1907 (1965).